ACS Photonics

Article

Cite This: ACS Photonics 2018, 5, 2609−2616

Plasmonic Enhanced EIT and Velocity Selective Optical Pumping Measurements with Atomic Vapor

Eliran Talker,[†] Pankaj Arora,[†] Yefim Barash, Liron Stern, and Uriel Levy*

Department of Applied Physics, The Benin School of Engineering and Computer Science, The Center for Nanoscience and Nanotechnology, The Hebrew University of Jerusalem, Jerusalem, 91904, Israel

Supporting Information

ABSTRACT: In this work, we experimentally observe for the first time nanoscale plasmonic enhanced Electromagnetically Induced Transparency (EIT) and Velocity Selective Optical Pumping (VSOP) effects in miniaturized Integrated Quantum Plasmonic Device (IQPD) for D_2 transitions in rubidium (Rb). Our device consists of a vapor cell integrated on top of a prism coated with a thin layer of metal. This configuration is known to allow efficient excitation of Surface Plasmon Resonance (SPR). The evanescent field of the surface plasmon mode interacts with the atomic media in close vicinity to the metal. In spite of the limited interaction length between SPR and Rb atoms, the signature of EIT along with VSOP signals could be clearly observed in our miniaturized IQPD under proper conditions of pump and probe intensities. A gradual decrease in the contrast of the plasmonic enhanced EIT and VSOP signals was observed as the excitation was detuned from the SPR critical angle, due to reduction in electromagnetic field enhancement, leading to a reduced interaction of the evanescent field with the atomic vapor media. Following the demonstration of these effects, we also present a detailed model revealing the mechanisms and the origin of plasmonic enhanced EIT and VSOP effects in our system. The model, which is based on the Bloch equations, is in good agreement with the observed experimental results. The obtained results are regarded as an important step in the quest for the realization of nanoscale quantum plasmonic effects and devices.

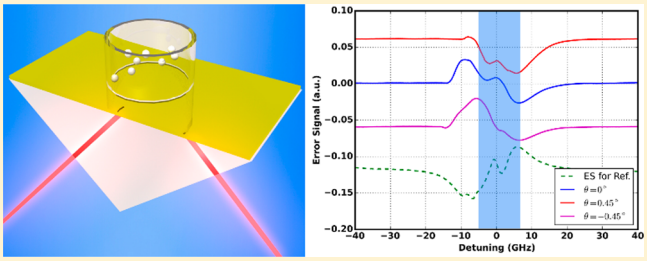

KEYWORDS: *surface plasmons, plasmon-atom interaction, quantum plasmonics, spectroscopy, atom optics*

The quantum interference due to coherent coupling between narrow and broad resonances leads to a sharp resonance of nearly perfect transmission known as Electromagnetically Induced Transparency (EIT). The EIT phenomenon is attracting growing attention due to its scientific merits as well as the potential applications, for example, in nonlinear optics, lasing without inversion, storage of light, ultraslow propagation, quantum memory, and quantum sensing, to name a few.[1−6] Motivated by the strong field localization and field enhancement, plasmonic and metamaterial nanostructures has been exploited to demonstrate EIT effects with high figure of merit in terms of narrow transparency and high modulation depth.[7−10] Traditionally, in the area of atomic physics, the principle of EIT is that an atomic coherence is induced in a multilevel system by a strong "pump" laser field which alters the response of the system to a "probe" laser field. The utmost simple level scheme for studying EIT features is that of the three level system[11] which can be classified into three categories: V-type, Lambda-type (Λ), and Cascade-type (Ξ). Yet, the study of EIT is not restricted to three level systems as evident, for example, by the plethora of EIT demonstrations in four-level[12−14] and even five level[15,16] systems. Observing EIT in V-type system is impossible for a cold V-type system because the quantum interference in such system is constructive. However, if the Doppler effect (for warm atomic or molecular gases) is taken into account, an EIT is possible and a crossover from EIT to Autler-Townes splitting can be observed.[17−20] For a typical V-type three level atomic system, the medium becomes transparent only at the centerline of the probe transition and no extra peaks are generated. However, in the case of multilevel (more than three levels) systems, due to the presence of extra upper levels with spacing smaller than the Doppler broadened transition, extra peaks, known as Velocity Selective Optical Pumping (VSOP) peaks, are also observed along with the EIT peak.[21−24] We will discuss these effects further in the text. We have chosen to focus on the V-type system rather than on the Lambda-type (Λ) or the Cascade-type (Ξ) systems because it is more difficult to observe the discussed effects in the V- type configuration. As such, it is the ideal system to make the case for plasmonics as it significantly enhancing VSOP and EIT effects, which may be difficult to observe in other, nonplasmonic miniaturized systems, such as total internal reflection glass prism with no metal coating.

In parallel, atomic spectroscopy in confined miniaturized cells[25−29] is a promptly emerging field with implications

Special Issue: Recent Developments and Applications of Plasmonics

Received: October 30, 2017
Published: January 25, 2018

DOI: 10.1021/acsphotonics.7b01284
ACS Photonics 2018, 5, 2609−2616

ranging from precision analysis of atomic structures to applications such as magnetometry,[30] optical and radio frequency standards,[31] and optical isolation.[32] Recent efforts are tailored toward the on-chip integration of atomic and nanophotonic systems, primarily motivated by the capability to enhance light−matter interactions at the nanometer scale.[33−37]

In this work, we report on an Integrated Quantum Plasmonic Device (IQPD) supporting the interactions of plasmons with atomic vapor at the nanoscale. This device is utilized to experimentally demonstrate plasmonic enhanced EIT and VSOP effects. Specifically, Surface Plasmon Resonance (SPR) is excited by a prism coated by a thin metallic film. While such system in which the excited Surface Plasmons (SPs) are interacting with atomic vapor of rubidium (Rb) via the evanescent tail of the plasmonic mode has been demonstrated before, primarily for the purpose of controlling dispersion, demonstrating Fano line shape and all-optical switching,[33] here we take advantage of such interactions and the significant field enhancement in order to demonstrate theoretically and experimentally for the first time EIT and VSOP effects in miniaturized vapor cells. The reported result can be regarded as an additional step in the quest for the realization of quantum plasmonic effects and devices.[38,39]

FABRICATION

The device was constructed on top of a right-angle CaF_2 prism. After cleaning with soap water and DI water, a stack of 3 nm chromium (as an adhesion layer), a 35 nm layer of gold and a 5 nm-thick layer of MgF_2 were evaporated on top of the prism at deposition rates of 0.3, 0.5, and 0.3 Å/s, respectively. The 5 nm thick MgF_2 layer on top of gold serves as a capping layer, to prevent chemical interaction between the gold and the Rb atoms. After evaporation, a Pyrex cell was bonded to the prism using thermally cured epoxy and baked out at a temperature of 70 °C for 3 h. The integrated device was baked out for 48 h using a turbo vacuum system which is connected to the cell until a vacuum level in the range of 10^{-7}−10^{-8} Torr was reached. Finally, a droplet of natural Rb was inserted into the cell which was prepared by condensation of Rb vapors in vacuum system connected to aluminosilicate glass ampule containing rubidium chloride (RbCl) and calcium (Ca), placed in high temperature oven. The Rb vapors were obtained by reduction of the RbCl with Ca.[40] The reduction reaction took place at elevated temperature, producing gaseous Rb which condensates on the cool walls of the glass system's main tube. Then it was transferred to the sample cell attached to the main tube, after which the cell was disconnected from the vacuum system and sealed. Figure 1a,b show the schematic and actual photograph of miniaturized IQPD filled with Rb atoms, respectively.

NUMERICAL PLASMONIC SIMULATIONS

The reflection and the electromagnetic field distribution in the bare plasmonic structure, prior to the introduction of Rb, were calculated using the transfer matrix method and Comsol Multiphysics, respectively. Here, the structure is represented by a glass prism with a refractive index of 1.4307, followed by metallic chromium and gold layers (refractive index of 3.9592 − *i*4.1936 and 0.18210 − *i*4.8493, respectively), and an MgF_2 capping layer with refractive index of 1.3753. This structure with air on top was used to calculate reflectivity curve of the SP mode as a function of the incident angle. Essentially, we assume

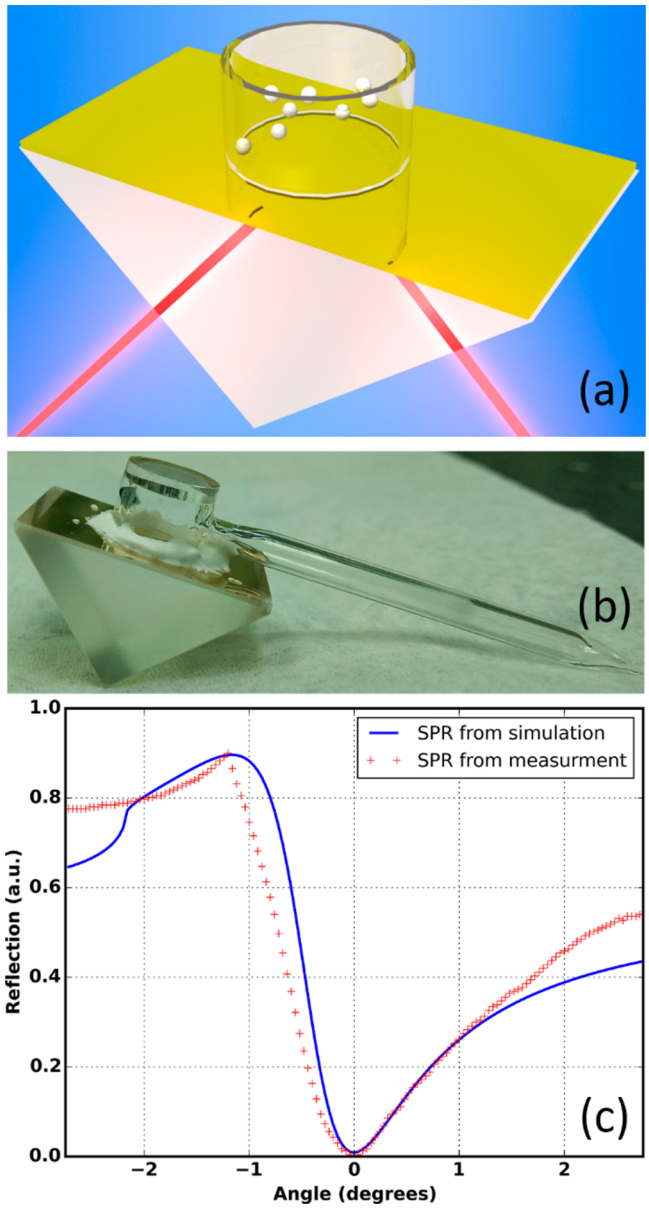

Figure 1. (a) Schematic and (b) photograph of miniaturized IQPD filled of Rb atoms. (c) Simulated and measured SP reflectivity curve for plasmonic prism as a function of incident angle.

the attenuated total internal reflection based Kretschmann configuration,[41] where the evanescent field from a Transverse Magnetic (TM) polarized light is coupled to SP mode around the critical resonance angle.

NUMERICAL RESULT

The simulated reflectivity of light at 780 nm through the plasmonic prism (not considering the effect of the Rb vapor) as a function of incident angle was calculated using the above-mentioned transfer matrix method. The result is shown in Figure 1c, solid blue line. The dip in reflection, which is attributed to the coupling of light to the SP mode, is obtained at an angle of 46.2°, which is defined as 0°. To compare the simulation with experiment data, a TM polarized light derived from 780 nm wavelength laser source (TOPTICA, DL pro) was used to excite IQPD, which was mounted on a rotation stage. The reflected signal was measured using a photodetector,

DOI: 10.1021/acsphotonics.7b01284
ACS Photonics 2018, 5, 2609−2616

while controlling the angle of the rotation stage over a wide range of angles spanning approximately ±3° around the plasmonic resonance with the angular resolution of 0.05°. The measured results are shown in Figure 1c, red dashed line. The reflectivity curves obtained from simulation and measurement were found in a good agreement.

MODELING THE INTEGRATED QUANTUM PLASMONIC DEVICE

Two major configurations can be applied to study light-atom interaction as shown in Figure 2a. One is the direct interaction

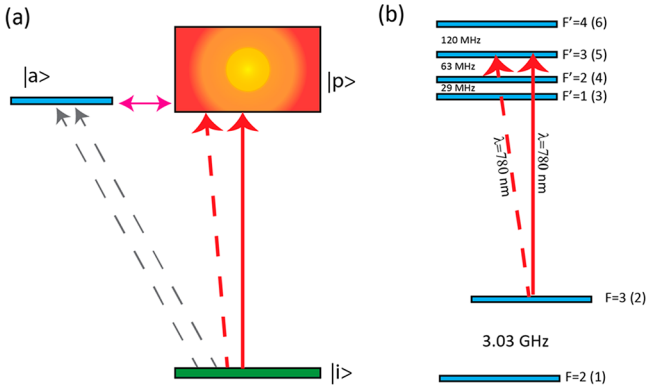

Figure 2. (a) Coupling mechanism in plasmonic-atomic hybrid system. |*i*> represents the incident light state, couples to the plasmonic state |*p*>. Then the plasmonic state |*p*> couples to discrete atomic state |*a*>. This is in contrast to the conventional light vapor interactions experiments, where direct light-atom coupling takes place by allowing the incident light state |*i*> to directly couple to an atomic state |*a*>. (b) Level scheme for ^{85}Rb-D_2 transition in V-type configuration.

of the incident light represented as $|i\rangle$ state with the atomic media represented as $|a\rangle$ state. Alternatively, the incident light state $|i\rangle$ is first coupled to a plasmonic state $|p\rangle$ and then the plasmonic state $|p\rangle$ couples to atomic state $|a\rangle$.[33,42] In this work, we are focused on the second case, i.e. plasmonic enhanced light-atom interaction (see Supporting Information, pages S1–S3) using our proposed IQPD device.

Next, we introduce the atomic media in details. The energy levels relevant for the observation of VSOP and EIT in our setup are shown in Figure 2b. We consider a six-level hyperfine structure of ^{85}Rb D_2 transition, where the energy levels are denoted as i = 1−6 and the spacing between the hyperfine splitting of the excited state is δ_1 = 29 *MHz*, δ_2 = 63 *MHz*, and δ_3 = 120 MHz, respectively.[43] In the considered V-type configuration, Level $|2\rangle$ is coupled to level $|5\rangle$ by the strong pump laser beam, and to levels $|4\rangle$, $|5\rangle$, and $|6\rangle$ by the weak probe laser beam. In a Doppler broadened system, the frequency detuning from the resonance of the pump and probe fields are defined as

$$\Delta_p = k_{pu}\cdot v$$
$$\Delta_c = k_{pr}\cdot v - \Delta \quad (1)$$

where v is the atomic velocity, Δ*i*s the detuning from resonance and k_{pu} and k_{pr} are the pump and probe wave-vectors, respectively. It should be noted that for zero detuning, there is still a residual Doppler line width $\Delta\nu_D$, which can be written for a V-type system as

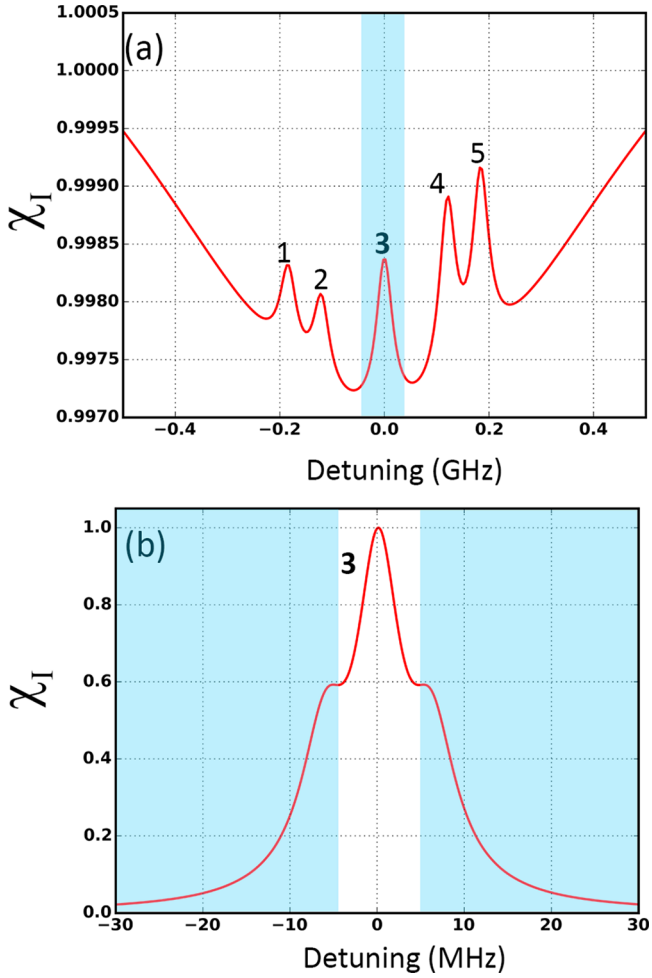

Figure 3. (a) Simulated normalized steady-state susceptibility of the six level atomic system. Temperature of 60 °C was assumed. The Rabi frequency for the pump and probe lasers were $\Omega_{pu} = 5\gamma$ and $\Omega_{pr} = 2\gamma$, respectively. The VSOP peaks can be clearly observed. (b) Zoom in on the 3rd VSOP peak, where the super imposed EIT peak can be observed.

$$\Delta\nu_D = |\vec{k}_{pu} - \vec{k}_{pr}|\cdot\vec{v}_p \quad (2)$$

where $\vec{v}_p$ is the most probable velocity of the atoms. This is equivalent to the case of nearly Doppler free environment due to using same wavelength in a nearly collinear configuration.[44]

To better understand the physical ground of this work, we have first calculated the optical susceptibility for a six-level quantum system of Rb atoms, where plasmonic effects are not present. Our theoretical calculations are based on a standard density matrix approach. The dynamical behavior of the density matrix ρ can be given by the Liouville equation of motion

$$\frac{d\rho}{dt} = -\frac{i}{\hbar}[\mathcal{H}, \rho] + \Gamma\rho \quad (3)$$

where Γ is the relaxation matrix, $\mathcal{H}$ is the Hamiltonian of the six-level atomic system including the electric dipole interaction and rotating wave approximation, which can be written as

$$\mathcal{H} = \mathcal{H}_0 + V_1 + V_2 = -\sum_{j=1}^{6} E_j|j\rangle\langle j| - \frac{\hbar}{2}\left[\sum_{j=4}^{6}\Omega_{pr}^{2j}(z)|2\rangle\langle j| + \Omega_{pu}^{25}(z)|2\rangle\langle 5|\right] \quad (4)$$

DOI: 10.1021/acsphotonics.7b01284
ACS Photonics 2018, 5, 2609−2616

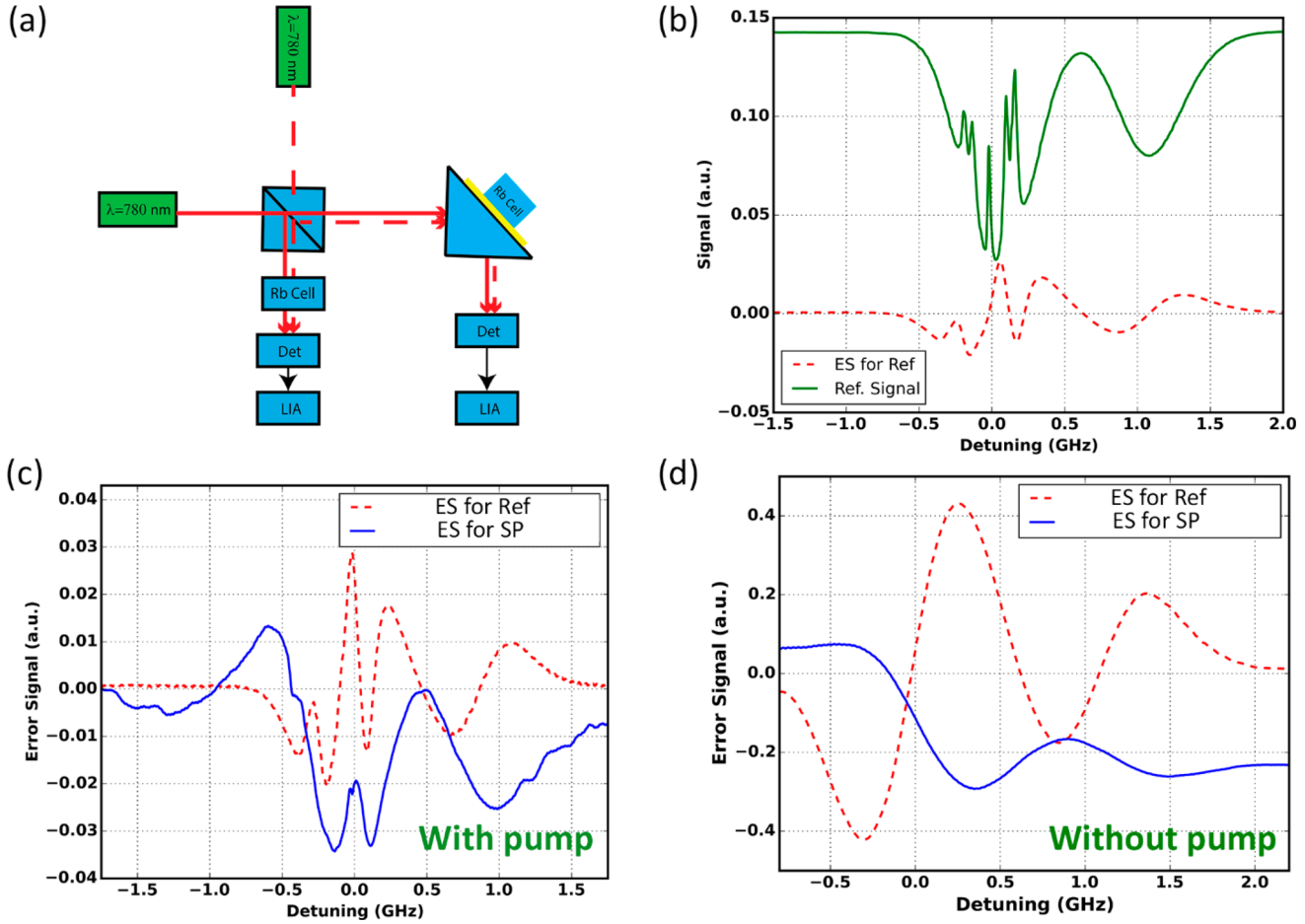

Figure 4. (a) Schematic description of the experimental setup. (b) Experimentally measured transmission and ES in the reference cell. (c, d) Experimentally measured ES in reference cell and IQPD with and without pump laser, respectively. The different normalization has been used for ES of reference cell and IQPD for visualization purposes during the experiments.

where E is the energy value of each level and $\Omega_{pu,pr}$ are the Rabi frequencies for the pump and probe beam, respectively, which can be written as

$$\Omega_{pu,pr} = -\frac{d\cdot \overrightarrow{E_{0,pu,pr}}}{\hbar} \tag{5}$$

Here d represents the dipole matrix and $\overrightarrow{E_{0,pu,pr}}$ represents the electric field for pump and probe, respectively. All the spontaneous emission rates of the excited states were presumed to be the same and all the ground level population relaxation rates were ignored under the assumption that the ground states are stable. We have assumed that the atomic density is sufficiently low to neglect the atom−atom interactions (collisional broadening). The bandwidth of the lasers was incorporated into the calculations by introducing relaxation terms for the nondiagonal density matrix elements using the procedure developed in ref 45.

As a result of applying this model, the imaginary part of the optical susceptibility $\chi_I(\Delta)$ related to the density matrix is plotted for the six-level atomic system, using following equation

$$\chi_I(\Delta) = -\frac{2\mathcal{N}}{\epsilon_0\hbar\Omega_{pr}} Im\sum_{i=4}^{6} d_{2,i}^2\rho_{2,i}(\Delta) \tag{6}$$

where $\mathcal{N}$ is the uniform number density for an atomic ensemble. The results are shown in Figure 3. The presence of five peaks corresponding to VSOP signal (solid red line) can be clearly observed in Figure 3a. These five peaks are labeled in the figure. The simulation represents a realistic experimental scenario, in which we measure the superimposed intensity of the pump and the probe beam. Basically, one should observe six peaks. Three are originated from changing the population distribution of the ground states due to velocity selective process. (The pump beam is set to $F = 3 \rightarrow F' = 3$ transition.) The Doppler shift causes the pump beam to interact with three groups of atoms: first group with velocity zero or perpendicular to the pump beam; therefore these atoms will be absorbed at frequency equals to $F = 3 \rightarrow F' = 3$ transition. Second and third groups of atoms should have a velocity that cause Doppler shift, fit for the transition $F = 3 \rightarrow F' = 2, 4$; the other three peaks are generated by the probe beam according to changing the population in the ground states by scanning the probe beam.[46] Yet, two of the peaks occur at the same frequency, and thus only five peaks are observed. Figure 3b shows a zoom in on the central peak labeled as third VSOP peak, and shaded by cyan rectangle in Figure 3a. Now, it is possible to observe an additional narrow peak (line width 8 MHz) on top of the third VSOP peak, which is attributed to the EIT effect. It should be noted that an EIT peak could be clearly observed in V-type configuration only if $\Omega_{pr} < \Omega_{pu}$ and $\Omega_{pu} \gg \gamma$ (see Supporting

DOI: 10.1021/acsphotonics.7b01284
ACS Photonics 2018, 5, 2609−2616

Information, pages S4–S6). In the simulation, we assumed $\Omega_{pu} = 5\gamma$, $\Omega_{pr} = 2\gamma$, whereas γ is the natural line width.

EXPERIMENTAL OBSERVATIONS IN THE INTEGRATED QUANTUM PLASMONIC DEVICE

After observing the signature of EIT and VSOP peaks in simulations, we turn into their experimental observation. Figure 4a shows the experimental set up used for observing these effects. Briefly, a high power, 780 nm (TOPTICA, DL pro) wavelength laser source (acts as a pump) and a lower power, 780 nm (New Focus, TLB-6700) wavelength laser source (acts as a probe) were combined (TM polarization), collimated, and copropagated toward the IQPD. The reflected signal was measured using a photodetector. After which, it was demodulated and amplified using lock-in amplifier (LIA, SRS model SR830), while scanning, at low frequency, the optical frequency of the laser across the absorption line. During the measurement, we only demodulated the weak probe beam, whereas the stronger pump beam remained constant without any frequency modulation. The LIA provides an Error Signal (ES), which is proportional to the derivative of the signal.

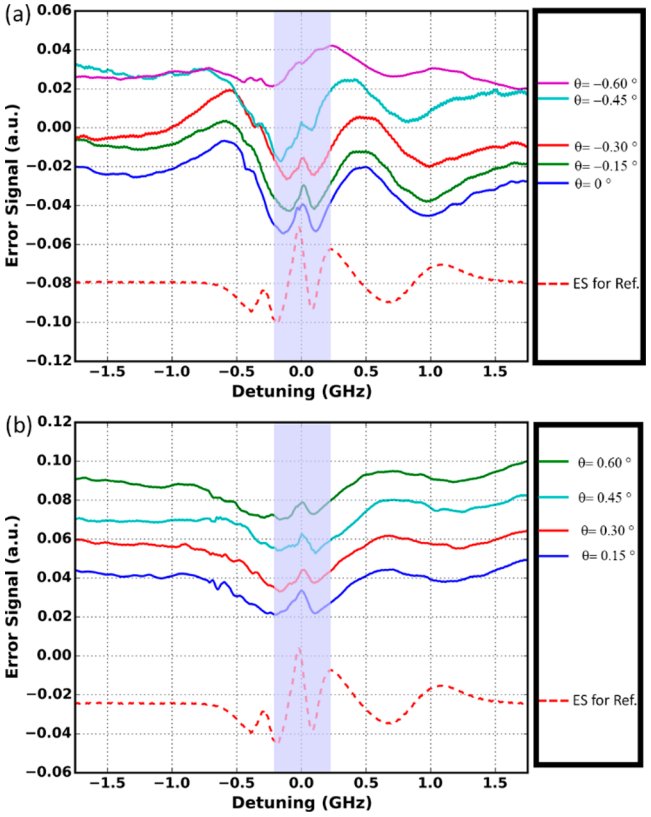

Figure 5. Experimentally measured ES for VSOP effect as a function of incident angles in IQPD: (a) In negative (left side from the resonance angle) direction; (b) In positive (right side from the resonance angle) direction.

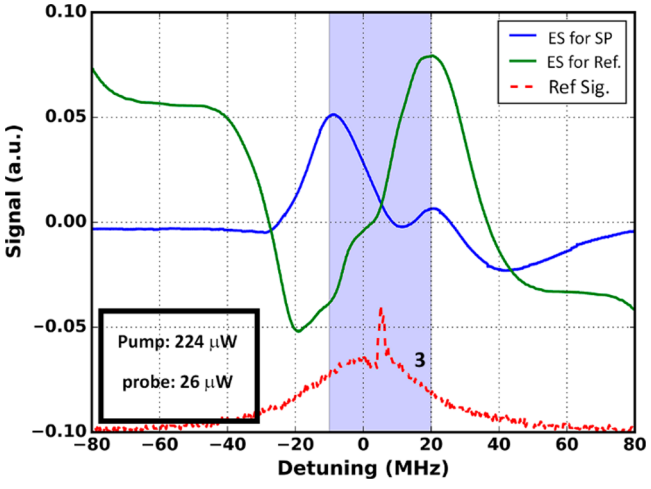

Figure 6. Experimental measured EIT signal in reference cell and IQPD.

In parallel, a beam splitter was also placed in the path of the copropagating light for the purpose of tapping some of the light and performing a parallel measurement using a 7.5 cm long reference vapor cell filled with natural Rb. The integrated device was heated using homemade resistive heaters and a temperature gradient was maintained during the experiment to avoid the adsorption of Rb atoms on the gold layer. The intensity of the incident light was controlled by Neutral Density filters.

The measured transmission curve for the 7.5 cm long reference cell is shown in Figure 4b (solid green line). The presence of the five peaks is clearly observed in agreement with the simulation results. We have also measured the ES which is proportional to the derivative of the signal with the help of the LIA, where the signature of VSOP peaks can also be seen (dashed red line). This ES is used as a reference for the purpose of comparison to the ES measured in the IQPD, as shown in the next paragraph.

After demonstrating the VSOP effects in the reference cell, we now focus on the study and the demonstration of these effects in our IQPD. Here, the interaction length of electromagnetic field with the atomic media is now significantly shorter as compared to the reference cell, resulting in a lower contrast, which can only be observed by extracting the ES. The ES of the reflection spectrum measured in our IQPD is shown in Figure 4c, blue line, with pump power of 137 μW and probe power of 42.5 μW, respectively. The VSOP effects can be clearly observed. One may observe that the ES of the IQPD is mostly negative, indicating VSOP dips rather than peaks, as was predicted and observed before.[28,40] To verify the presence of VSOP signal, we have blocked the pump laser such that the sample was excited only by the probe laser in both the reference cell and the IQPD. Figure 4d shows the ES for the reference cell and the IQPD without the presence of the pump laser. The absence of VSOP signal serves as a control experiment and supports the claim that the signal shown in Figure 4c is indeed originating from the VSOP effect.

After observing the VSOP signature in the IQPD, we have repeated the measurements, this time while controlling the angle of incidence as shown in Figure 5. As can be seen, by detuning away from the angle of plasmonic resonance, a gradual decrease in the contrast of VSOP signal is observed. This is because when the angle of incidence is detuned from resonance, the electromagnetic field enhancement at the metal-vapor interface is gradually decreased, and correspondingly the interaction between SP mode and atomic vapors is reduced as well. By comparing Figure 5a to Figure 5b, one may observe that the decrease in the contrast of VSOP signal is not symmetric. This is due to the asymmetric nature of the excited SP mode (see Figure 1c).

DOI: 10.1021/acsphotonics.7b01284
ACS Photonics 2018, 5, 2609–2616

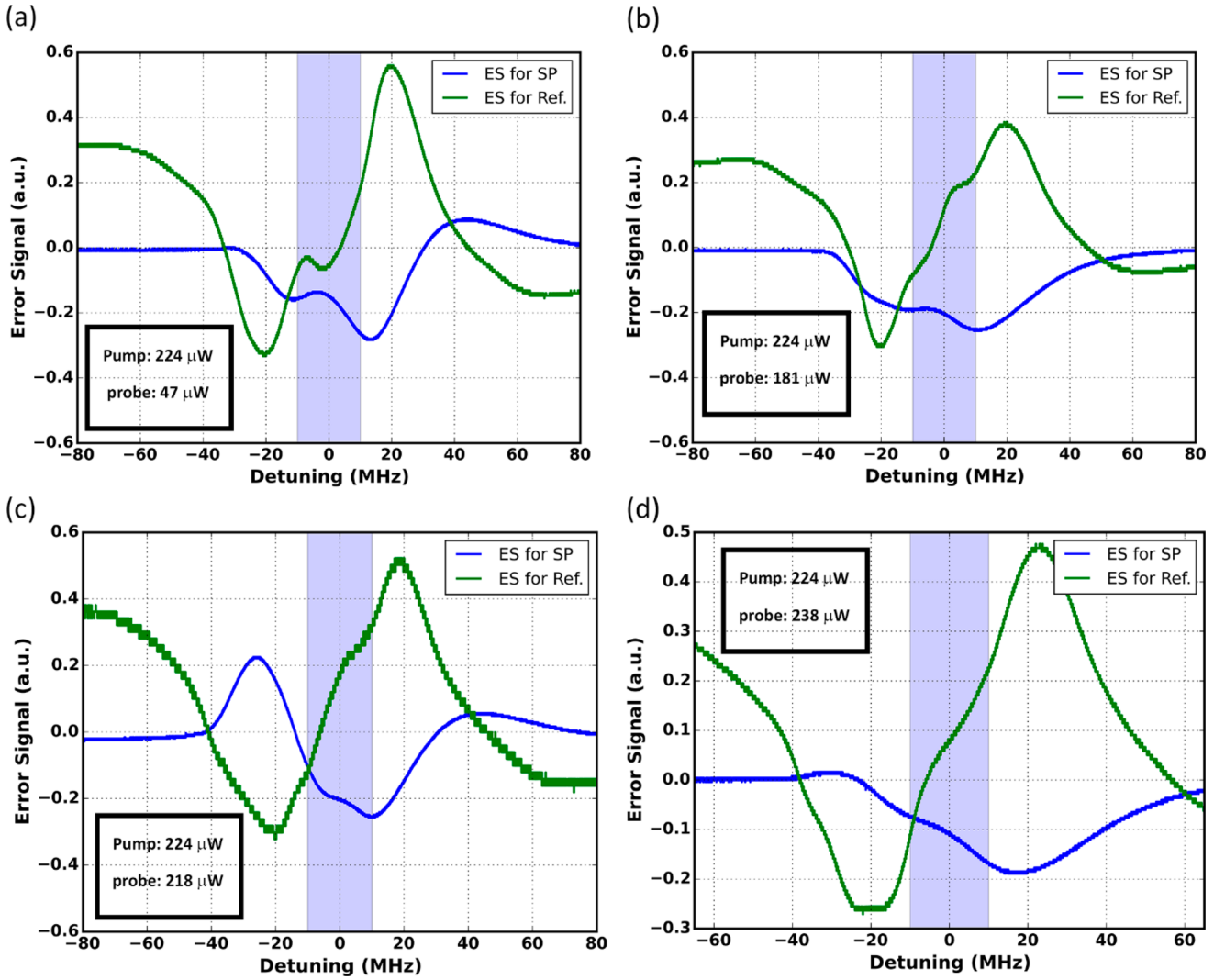

Figure 7. EIT spectrum in the reference cell and in our IQPD for various probe powers (a) 47, (b) 181, (c) 218, and (d) 238 μw, respectively. For comparison purposes, error signal (ES) has been used for both the reference cell and the IQPD in all four panels.

Next, we have focused on the experimental observation of EIT feature in the reference cell and IQPD, as shown in Figure 6. This time, we measured over a limited spectral band of about 160 MHz with increased pump power of 224 μw in order to improve the signal contrast. By zooming in on the third VSOP peak region and choosing pump power of 224 μW and probe power of 26 μW, respectively, we could now observe an EIT signal in the reference Rb cell (dashed red line), which appears as a sharp peak on top of third broader VSOP peak (Figure 6). The observed EIT signal was noticed to be a bit asymmetric and not perfectly centered as compared to simulation result (Figure 3b). This is probably due to a small detuning of the pump beam during the experiment. The green and blue lines are the ES of the reference cell and IQPD respectively, where the signature of EIT signal is clearly observed in both cases. As can be seen, the change in the ES around the EIT spectral regime (corresponding to a variation in the derivative of the signal) is limited to a narrow frequency regime as compared to the ES of the VSOP. Thus, it is evident that the line width for EIT signal is significantly narrower than the line width of VSOP signal in both the reference cell and the IQPD, in agreement with previously demonstrated results.[23,24] Comparing the line width of the EIT feature observed in the IQPD system to the reference signal, the feature was found to be broader in our IQPD system. This is attributed to transit time broadening in our plasmonic system.

After observing the EIT signal in the IQPD, the power for the probe laser was gradually increased to see its effect on the EIT signal. The pump power was kept constant (224 μw).

As the probe power was increased from 47 μw to 181 μw, as shown in Figure 7a and b, respectively, the decrease in the contrast of EIT signal was noticed in both reference cell and the IQPD. When the probe power was further increased toward the power level of the pump beam (Figure 7c,d), the signature of EIT signal could not be observed. This is due to the fact that the required pump−probe condition for observation of EIT is no longer fulfilled, as was previously discussed in Figure 3b.

Finally, to demonstrate the role of plasmons in enhancing the EIT signal in our IQPD, we have measured the ES while tuning the angle of incidence, using pump power of 224 μW and probe power of 26 μW, respectively, during the experiment. The obtained results are shown in Figure 8. As in the case of VSOP, one can clearly observe that as the angle of incidence is further detuned from the plasmonic resonance, a gradual decrease in the contrast of the EIT signal is observed. Again, this can be explained by the gradual decrease in field enhancement, as

DOI: 10.1021/acsphotonics.7b01284
ACS Photonics 2018, 5, 2609−2616

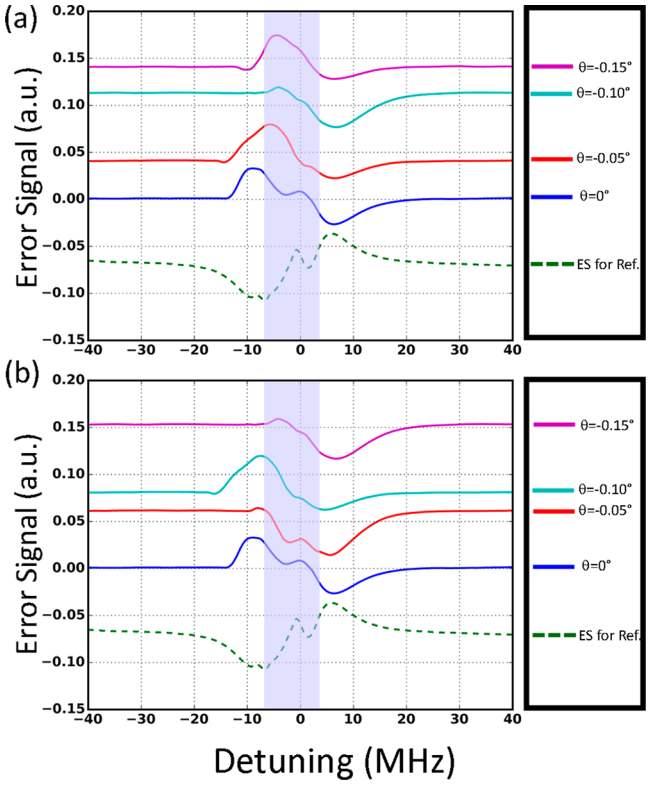

Figure 8. Experimental measured ES for EIT effect as a function of incident angle in IQPD: (a) In negative (Left side from the resonance angle) direction; (b) In positive (right side from the resonance angle) direction.

discussed in Figure S2 of the Supporting Information. In fact, the utilization of plasmonic effects is beneficial not only from miniaturization and field enhancement perspective, but also from the perspective of lifetime shortening, which assists in diminishing other mechanisms such as optical pumping which may compete with the EIT effect.

CONCLUSIONS

In this work, we have observed plasmonic enhanced Velocity Selective Optical Pumping (VSOP) and Electromagnetic Induced Transparency (EIT) signals in a miniaturized Integrated Quantum Plasmonic Device (IQPD). The device is realized by the integration of metal coated prism with atomic vapor media. The results were obtained under different conditions of pump and probe intensities, and under different detuning conditions from the critical angle for surface plasmon resonance (SPR). We observed a gradual increase in the contrast of nanoscale plasmonic enhanced VSOP and EIT signals as the angle of incidence approaches the critical SPR angle. This is attributed to the plasmonic field enhancement in the vicinity of the metal−vapor interface. We have also observed an increase in EIT contrast by increasing the intensity ratio between the pump and the probe. To support our experimental observations, we have calculated the expected signal in our system using numerical simulations based on the optical Bloch equation. The calculated effect was found to be in good agreement with the observed experimental results. Our IQPD and its functionality can be regarded as an additional step in the quest for the realization of nanoscale quantum plasmonic effects and devices. While ohmic loss results in the broadening of the plasmonic resonance, the effect of field enhancement provides valuable features compensating for such broadening. In future work, we intend to replace the metal film with plasmonic nanostructures such as nanoantennas. While ohmic loss will still play a role, we will benefit from even more extreme light confinement and field enhancement which is expected to make the plasmonic-atomic EIT more attractive for practical applications.

ASSOCIATED CONTENT

Supporting Information

The Supporting Information is available free of charge on the ACS Publications website at DOI: 10.1021/acsphotonics.7b01284.

Plasmonic enhancement in EIT and VSOP features; V type configuration for observing EIT features (PDF).

AUTHOR INFORMATION

Corresponding Author

*E-mail: ulevy@mail.huji.ac.il.

ORCID

Pankaj Arora: 0000-0002-0451-9518

Uriel Levy: 0000-0002-5918-1876

Author Contributions

†E.T. and P.A. contributed equally to this work.

Notes

The authors declare no competing financial interest.

ACKNOWLEDGMENTS

We acknowledge financial support from the ERC Project Light−Vapor Interactions on a chip (LIVIN).

REFERENCES

(1) Harris, S. E.; Field, J. E.; Imamoglu, A. Nonlinear Optical Processes Using Electromagnetically Induced Transparency. *Phys. Rev. Lett.* **1990**, *64*, 1107−1110.

(2) Abel, R. P.; Mohapatra, A. K.; Bason, M. G.; Pritchard, J. D.; Weatherill, K. J.; Raitzsch, U. Laser Frequency Stabilization to Excited State Transitions Using Electromagnetically Induced Transparency in a Cascade System. *Appl. Phys. Lett.* **2009**, *94*, 071107.

(3) Phillips, D. F.; Fleischhauer, A.; Mair, A.; Walsworth, R. L. Storage of Light in Atomic Vapor. *Phys. Rev. Lett.* **2001**, *86*, 783−786.

(4) Shuker, M.; Firstenberg, O.; Pugatch, R.; Ron, A.; Davidson, N. Storing Images in Warm Atomic Vapor. *Phys. Rev. Lett.* **2008**, *100*, 223601.

(5) Harris, S. E. Lasers without Inversion: Interference of Lifetime-Broadened Resonances. *Phys. Rev. Lett.* **1989**, *62*, 1033−1036.

(6) Liu, C.; Dutton, Z.; Behroozi, C. H.; Hau, L. V. Observation of Coherent Optical Information Storage in an Atomic Medium Using Halted Light Pulses. *Nature* **2001**, *409*, 490−493.

(7) Zhang, S.; Genov, D. A.; Wang, Y.; Liu, M.; Zhang, X. Plasmon-Induced Transparency in Metamaterials. *Phys. Rev. Lett.* **2008**, *101*, 47401.

(8) Dong, Z.; Liu, H.; Cao, J.; Li, T.; Wang, S.; Zhu, S.; Zhang, X. Enhanced Sensing Performance by the Plasmonic Analog of Electromagnetically Induced Transparency in Active Metamaterials. *Appl. Phys. Lett.* **2010**, *97*, 114101.

(9) Liu, N.; Langguth, L.; Weiss, T.; Kastel, J.; Fleischhauer, M.; Pfau, T.; Giessen, H. Plasmonic Analogue of Electromagnetically Induced Transparency at the Drude Damping Limit. *Nat. Mater.* **2009**, *8*, 758−762.

(10) Wu, D.; Liu, Y.; Yu, L.; Yu, Z.; Chen, L.; Li, R.; Ma, R.; Liu, C. Plasmonic Metamaterial for Electromagnetically Induced Transparency Analogue and Ultra- High Figure of Merit Sensor. *Sci. Rep.* **2017**, *7*, 45210.

DOI: 10.1021/acsphotonics.7b01284
ACS Photonics 2018, 5, 2609−2616

(11) Li, Y.; Jin, S.; Xiao, M. Observation of an Electromagnetically Induced Change of Absorption in Multilevel Rubidium Atoms. *Phys. Rev. A: At., Mol., Opt. Phys.* **1995**, *51*, 1754−1757.
(12) Agarwal, G. S.; Harshawardhan, W. Inhibition and Enhancement of Two Photon Absorption. *Phys. Rev. Lett.* **1996**, *77*, 1039−1042.
(13) McGloin, D. Coherent Effects in a Driven Vee Scheme. *J. Phys. B: At., Mol. Opt. Phys.* **2003**, *36*, 2861−2871.
(14) Lukin, M. D.; Imamoglu, A. Controlling Photons Using Electromagnetically Induced Transparency. *Nature* **2001**, *413*, 273−276.
(15) Ottaviani, C.; Rebic, S.; Vitali, D.; Tombesi, P. Quantum Phase-Gate Operation Based on Nonlinear Optics: Full Quantum Analysis. *Phys. Rev. A: At., Mol., Opt. Phys.* **2006**, *73*, 10301.
(16) Wu, Y.; Saldana, J.; Zhu, Y. Large Enhancement of Four-Wave Mixing by Suppression of Photon Absorption from Electromagnetically Induced Transparency. *Phys. Rev. A: At., Mol., Opt. Phys.* **2003**, *67*, 13811.
(17) Agarwal, G. S. Nature of the Quantum Interference in Electromagnetic-Field-Induced Control of Absorption. *Phys. Rev. A: At., Mol., Opt. Phys.* **1997**, *55*, 2467−2470.
(18) Anisimov, P.; Kocharovskaya, O. Decaying-Dressed-State Analysis of a Coherently Driven Three-Level System. *J. Mod. Opt.* **2008**, *55*, 3159−3171.
(19) Abi-Salloum, T. Y. Electromagnetically Induced Transparency and Autler-Townes Splitting: Two Similar but Distinct Phenomena in Two Categories of Three-Level Atomic Systems. *Phys. Rev. A: At., Mol., Opt. Phys.* **2010**, *81*.10.1103/PhysRevA.81.053836
(20) Zhu, C.; Tan, C.; Huang, G. Crossover from Electromagnetically Induced Transparency to Autler-Townes Splitting in Open V-Type Molecular Systems. *Phys. Rev. A: At., Mol., Opt. Phys.* **2013**, *87*, 1−13.
(21) Bhattacharyya, D.; Ray, B.; Ghosh, P. N. Theoretical Study of Electromagnetically Induced Transparency in a Five-Level Atom and Application to Doppler-Broadened and Doppler-Free Rb Atoms. *J. Phys. B: At., Mol. Opt. Phys.* **2007**, *40*, 4061−4075.
(22) Ying, K.; Niu, Y.; Chen, D.; Cai, H.; Qu, R. Observation of Multi-Electromagnetically Induced Transparency in V-Type Rubidium Atoms. *J. Mod. Opt.* **2014**, *61*, 631−635.
(23) Bhattacharyya, D.; Ghosh, A.; Bandyopadhyay, A.; Saha, S.; Sankar De. Comparison of Electromagnetically Induced Transparency (EIT) Spectra for Six-Level Lambda (Λ) and Five-Level V-Type Systems. *J. Atomic, Mol., Condens. Nano Phys.* **2015**, *2*, 93−99.
(24) Mitra, S.; Dey, S.; Hossain, M. M.; Ghosh, P. N.; Ray, B. Temperature and Magnetic Field Effects on the Coherent and Saturating Resonances in Λ- and V-Type Systems for the 85Rb-D2 Transition. *J. Phys. B: At., Mol. Opt. Phys.* **2013**, *46*, 75002.
(25) Schwindt, P. D. D.; Knappe, S.; Shah, V.; Hollberg, L.; Kitching, J.; Liew, L.; Moreland, J.; Schwindt, P. D. D.; Knappe, S.; Shah, V.; et al. Chip-Scale Atomic Magnetometer. *Appl. Phys. Lett.* **2004**, *85*, 6409−6411.
(26) Benabid, F.; Couny, F.; Knight, J. C.; Birks, T. A.; Russell, P. S. J. Compact, Stable and Efficient All-Fibre Gas Cells Using Hollow-Core Photonic Crystal Fibres. *Nature* **2005**, *434*, 488.
(27) Yang, W.; Conkey, D. B.; Wu, B. I. N.; Yin, D.; Hawkins, A. R.; Schmidt, H. Atomic Spectroscopy on a Chip. *Nat. Photonics* **2007**, *1*, 331−335.
(28) Baluktsian, T.; Urban, C.; Bublat, T.; Giessen, H.; Löw, R.; Pfau, T. Fabrication Method for Microscopic Vapor Cells for Alkali Atoms. *Opt. Lett.* **2010**, *35*, 1950−1952.
(29) Sargsyan, A.; Leroy, C.; Pashayan-Leroy, Y.; Mirzoyan, R.; Papoyan, A.; Sarkisyan, D. High Contrast D 1 Line Electromagnetically Induced Transparency in Nanometric-Thin Rubidium Vapor Cell. *Appl. Phys. B: Lasers Opt.* **2011**, *105*, 767−774.
(30) Kominis, I. K.; Kornack, T. W.; Allred, J. C.; Romalis, M. V. A Subfemtotesla Multichannel Atomic Magnetometer. *Nature* **2003**, *422*, 596−599.
(31) Venkataraman, V.; Saha, K.; Londero, P.; Gaeta, A. L. Few-Photon All-Optical Modulation in a Photonic Band-Gap Fiber. *Phys. Rev. Lett.* **2011**, *107*, 193902.
(32) Salit, K.; Salit, M.; Krishnamurthy, S.; Wang, Y.; Kumar, P.; Shahriar, M. S. High Bandwidth, Ultra-Low Power All Optical Modulation with a Nano-Fiber Embedded in Rb Vapor. *OSA CLEO* **2010**, 1−2.
(33) Stern, L.; Grajower, M.; Levy, U. Fano Resonances and All-Optical Switching in a Resonantly Coupled Plasmonic−atomic System. *Nat. Commun.* **2014**, *5*, 1−9.
(34) Stern, L.; Zektzer, R.; Mazurski, N.; Levy, U. Enhanced Light-Vapor Interactions and All Optical Switching in a Chip Scale Micro-Ring Resonator Coupled with Atomic Vapor. *Laser and Photonics Reviews* **2016**, *10*, 1−7.
(35) Stern, L.; Desiatov, B.; Mazurski, N.; Levy, U. Strong Coupling and High-Contrast All-Optical Modulation in Atomic Cladding Waveguides. *Nat. Commun.* **2017**, *8*, 1−7.
(36) Ritter, R.; Gruhler, N.; Pernice, W.; Kübler, H.; Pfau, T.; Löw, R.; Pfau, T. Atomic Vapor Spectroscopy in Integrated Photonic Structures Atomic Vapor Spectroscopy in Integrated Photonic Structures. *Appl. Phys. Lett.* **2015**, *10*741101.10.1063/1.4927172
(37) Aljunid, S. A.; Chan, E. A.; Adamo, G.; Ducloy, M.; Wilkowski, D.; Zheludev, N. I. Atomic Response in the Near-Field of Nanostructured Plasmonic Metamaterial. *Nano Lett.* **2016**, *16*, 3137−3141.
(38) Kulkarni, V.; Prodan, E.; Nordlander, P. Quantum Plasmonics: Optical Properties of a Nanomatryushka. *Nano Lett.* **2013**, *13*, 5873−5879.
(39) Esteban, R.; Borisov, A. G.; Nordlander, P.; Aizpurua, J. Bridging Quantum and Classical Plasmonics with a Quantum-Corrected Model. *Nat. Commun.* **2012**, *3*, 1−9.
(40) Hevl, L. H. *Chim. Acta* **1928**, *11*, 1008.
(41) Homola, J.; Yee, S. S.; Gauglitz, G. Surface Plasmon Resonance Sensors. *Sens. Actuators, B* **1999**, *54*, 3−15.
(42) Giannini, V.; Francescato, Y.; Amrania, H.; Phillips, C. C.; Maier, S. A. Fano Resonances in Nanoscale Plasmonic Systems: A Parameter-Free Modeling Approach. *Nano Lett.* **2011**, *11*, 2835−2840.
(43) Steck, D. A. Rubidium 85 D Line Data; http://www.opencontent.org/openpub/.
(44) Fulton, D. J.; Shepherd, S.; Moseley, R. R.; Sinclair, B. D.; Dunn, M. H. Continuous-Wave Electromagnetically Induced Transparency: A Comparison of V, A, and Cascade Systems. *Phys. Rev. A: At., Mol., Opt. Phys.* **1995**, *52*, 2302−2311.
(45) Purves, G. T. *Absorption And Dispersion In Atomic Vapours: Applications To Interferometery*; Durham University, 2006.
(46) Rehman, H. U.; Noh, H.-R.; Kim, J.-T. Velocity Selective Optical Pumping Effects on 85Rb Atoms from Various Coupling Beam Polarization Configurations. *Opt. Commun.* **2017**, *402*, 567−571.

DOI: 10.1021/acsphotonics.7b01284
ACS Photonics 2018, 5, 2609−2616